Journal of Thermal Analysis, Vol. 48 (1997) 1051-1067

THERMOANALYTICAL INVESTIGATIONS ON THE SOL-GEL SYNTHESIS OF $YBa_2Cu_3O_{7-\delta}$

G. V. Rama Rao, U. V. Varadaraju, S. Venkadesan and S. L. Mannan*

Materials Development Division, Indira Gandhi Centre for Atomic Research, Kalpakkam 603 102
*Materials Science Research Centre, Indian Institute of Technology, Madras 600 036, India

Abstract

The high temperature superconducting compound $YBa_2Cu_3O_{7-\delta}$ (Y-123) is synthesised by sol-gel process using various precursors viz., acetate, acetate-citrate, nitrate-citrate and acrylamide. The phase purity of the final product depends on the homogeneity of the gels which intern depends on the bonding of the metal ions in the gels. The samples prepared by acrylamide and nitrate-citrate gel routes yielded phase pure Y-123 compound with better superconducting properties. The mechanism of formation of Y-123 in all these four gel routes is established by characterising the gels and intermediate phases using TG, DTA and XRD techniques. Kinetic analysis is carried out on the mass loss data using the method proposed by Phadni's and Deshpande. Avrami-Erofeev nuclei growth in case of acrylamide, diffusion controlled process in nitrate-citrate and phase boundary reaction mechanisms in case of acetate-citrate gels are found to be responsible for the formation of Y-123 phase.

Keywords: reaction mechanisms, sol-gel, superconductors, thermoanalytical techniques

Introduction

The high-temperature superconducting compound $YBa_2Cu_3O_{7-\delta}$ (Y-123) can be prepared in several ways, including the solid state, nitrate, co-precipitation and sol-gel routes using various starting materials [1–6]. The method of synthesis and subsequent heat treatment schedules are of great importance in the preparation of high quality superconductors. To standardise the conditions of preparation, the study of the kinetics and the reaction mechanism of formation of Y-123 is essential. Thermal analysis is one of the most versatile techniques used in ceramic oxide superconductor research and its application is widely quoted since the discovery of high temperature oxide superconductors [7–10].

Several reports appeared on the kinetics and mechanism of Y-123 compound prepared through solid state route [7, 11–14]. Even with the same experimental techniques and evaluation procedure the difference in activation energies for the reactions of solid state route is enormous. The kinetics of CO_2 evolution from $BaCO_3$ in the feed oxide mixture is more complicated. The value of activation energy changes depending on the fraction reacted α. The change probably arises owing to

0368–4466/97/ $ 5.00

John Wiley & Sons Limited
Chichester

the change in the reaction pathway and the influence of processes which take place simultaneously with CO_2 evolution [7]. This indicates the complexity of the reaction involved. This may be due to slow reaction rates that usually take place in the solid state reactions.

Sol-gel process is identified in the literature as one of the most promising techniques for the synthesis of superconductors for its ability to produce fine and homogeneous powders [15, 16]. Various precursors are employed to synthesise Y-123 compound by sol-gel process. The quality assurance of the final product is dependent on the homogeneity and bonding behaviour of the metal complexes within the gel. Reports on the kinetics and mechanism of formation of Y-123 by sol-gel route [17] are very scarce. In an earlier paper, we reported on the influence of various gel routes (viz., acetate, acetate-citrate, nitrate-citrate and acrylamide) on the synthesis of Y-123 compound by correlating the bonding behaviour of metal ions in the gels to the phase purity of the final product [5]. In this paper, the kinetics and mechanism of formation of Y-123 through various gel routes are presented. Thermogravimetry and differential thermal analytical and XRD techniques are employed to study the mechanism of formation of Y-123 compound through the different gel routes namely acetate, acetate-citrate, nitrate-citrate and acrylamide.

Experimental

Gels are prepared by acetate, acetate-citrate, nitrate-citrate and acrylamide gel routes. The preparation of gel samples is described elsewhere [5]. The gels are decomposed at 673–823 K and powders thus obtained are heat treated at 1173 K/24 h in air. Powders are compacted at 300 MPa and sintered at 1173 K/24 h in oxygen and are slowly cooled to room temperature. Samples are characterised by XRD after every heat treatment. TG and DTA (Polymer STA 1500) studies are carried out in the range 300 to 1248 K following a heating rate of 8 K min^{-1}. In order to supplement the thermoanalytical data and to find out the intermediate phases during the formation of Y-123, samples are heat treated to various temperatures following the same heating rate as that of thermal runs and are air quenched from their respective temperatures. Particle size measurements are carried out on precursor powders and Y-123 powders using Malvern Zeta Sizer-2 and Malvern E3600 particle sizer respectively. Resistivity measurements are carried out on sintered pellets using vander Pauw four probe method.

Results and discussion

Phase formation

The TG curves and DTA patterns of all the gel samples are shown in Figs 1 and 2 respectively. The inception and peak temperatures obtained from DTA patterns are given in Table 1. In case of the acetate gel, a continuous mass loss is observed in the temperature range of 513–693 K. A strong exotherm at 630 K and two weak exotherms at 513 and 570 K are observed from the DTA patterns. The strong

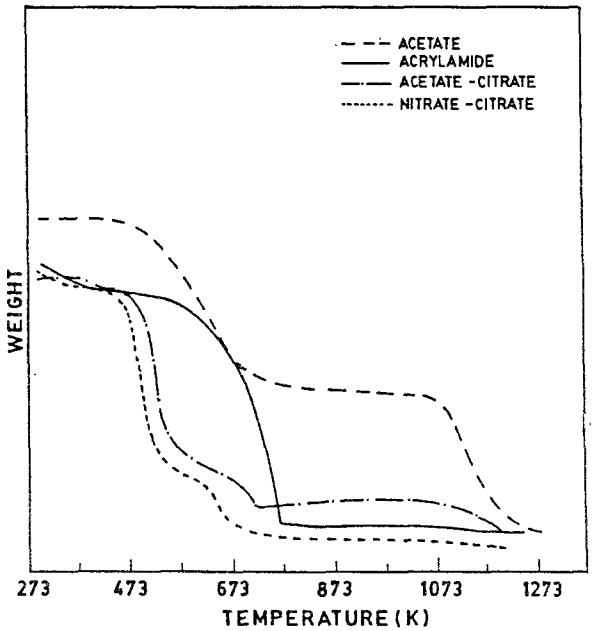

Fig. 1 TG patterns of various gels showing the mass loss during decomposition

exotherm is attributed to the decomposition of metal acetate network formed in the gel and the weak exotherms to the decomposition of copper acetate and yttrium acetate. It appears that some part of the copper acetate and yttrium acetate did not participate in the metal carboxylate network in the gel.

The acetate-citrate gel clearly shows two step mass loss during the decomposition of the gel in the range 467–548 K, 605–724 K and the corresponding DTA peaks are observed at 513 and 658 K. The exotherm at 513 K is attributed to the decomposition of copper acetate and the one at 658 K to the decomposition of the gel. The presence of the exotherm at 513 K, similar to the one reported for acetate gel indicates that copper acetate is not fully participating in the acetate-citrate gel.

In the case of the nitrate-citrate gel, the decomposition of the gel is divided into two steps (a) 450–540 K and (b) 615–696 K. Correspondingly three exothermic peaks appeared with their inception temperatures at 468, 524 and 600 K. Since these peaks are exothermic in nature, they can not be attributed to the decomposition of metal nitrates because nitrates decompose endothermically and rather at higher temperatures. It is obvious that metal ions are complexed with citric acid and the exothermic peaks are due to the decomposition of the complexes.

The mass loss is continuous from 573–773 K during the decomposition of acryl-amide gel. The appearance of a single strong exothermic peak in DTA at 683 K suggest that the metal ions are homogeneously distributed in the acrylamide polymeric network.

Thus, thermal analyses of gel samples show that, except for the acrylamide gel, all the other gels contain some quantities of individual metal carboxylates. The re-

sults of thermal analyses corroborates well with the results from IR, electronic and ESR spectral studies [5].

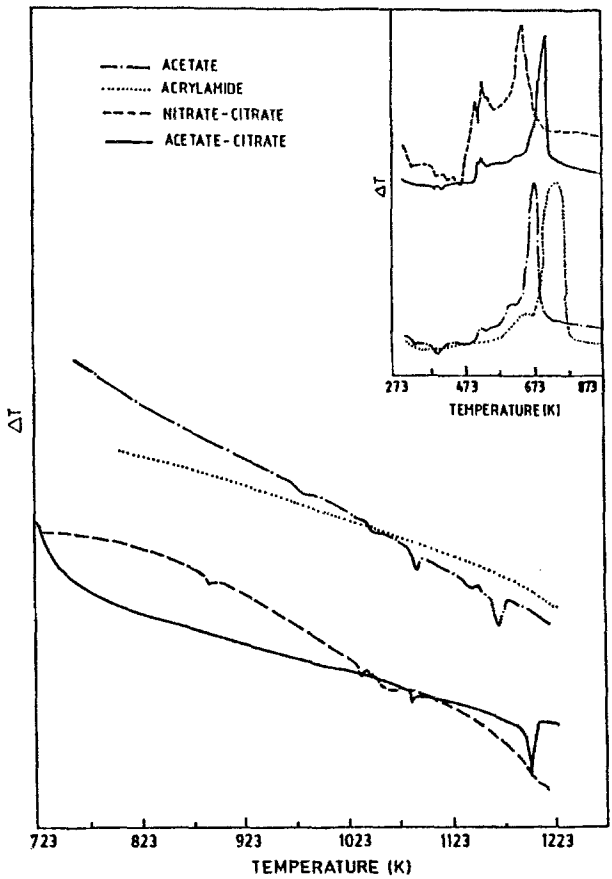

Fig. 2 DTA patterns of various gel samples in expanded scale; the inset show exotherms corresponding to gel decomposition

Table 1 Inception and peak temperatures (K) of endotherms and exotherms from DTA patterns of gel samples derived from various routes

S. No.	Acrylamide		Nitrate-citrate		Acetate-citrate		Acetate	
	i	p	i	p	i	p	i	p
1. exo	559 (sh)	578 (sh)	468	516	497	531	513	523
2. exo	683	744	524 (sh)	534 (sh)	599 (sh)	635 (sh)	570	618
3. exo	–	–	600	650	658	717	630	685
4. endo	–	–	–	1083	1080	1086	1083	1095
5. endo	–	–	–	–	1188	1197	1151	1166

i=inception temperature, p=peak temperature and sh=shoulder.

The decomposition temperatures of the gels are identified from the TG data. The XRD patterns of the samples quenched from the gel decomposition temperatures are shown in Fig. 3. The samples prepared by acetate and acetate-citrate gel routes contain Y_2O_3, $BaCO_3$ and CuO phases at the gel decomposition temperature. The formation of Y-123 initiates at gel decomposition temperature itself in case of acrylamide gel. Whereas, $BaCuO_2$ phase formation is observed in the nitrate-citrate gels when heat treated at 773 K/5 h but the phases formed at gel decomposition temperature are similar to that of acetate and acetate-citrate gels. In the present study the endothermic peak around 1078 K (Fig. 2) is due to the phase transition of $BaCO_3$ from rhombic to hexagonal [18]. This phase transition peak is not observed in acrylamide gel samples and in nitrate-citrate samples while an endotherm is observed for acetate and acetate-citrate gel samples. The endothermic peak around 1183 K in acetate and acetate-citrate gel samples is attributed to the phase formation of Y-123 whereas a corresponding peak is not observed for nitrate-citrate and acrylamide gel samples. The absence of the phase transformation peak of $BaCO_3$ at around 1083 K in acrylamide and nitrate-citrate gel samples indicates that the reac-

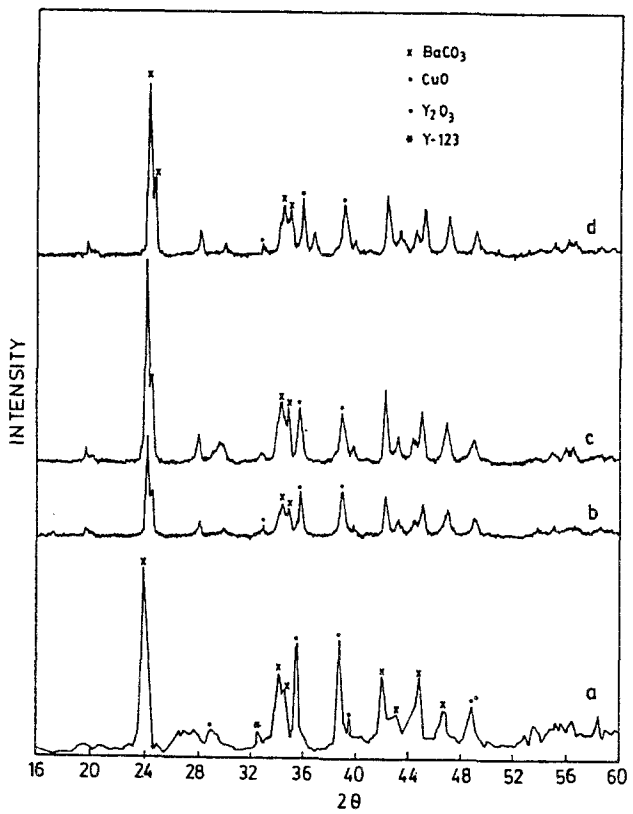

Fig. 3 XRD patterns of the samples quenched at gel decomposition temperatures (K) showing the formation of various phases a) acrylamide (778), b) acetate (698), c) acetate-citrate (724) and d) nitrate-citrate (698)

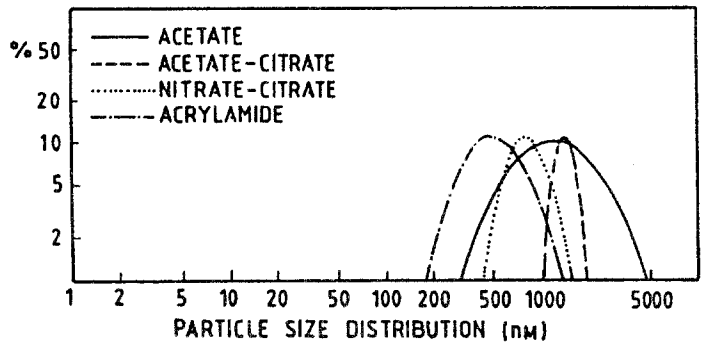

Fig. 4 Particle size distribution of precursor powders obtained on gel decomposition. Submicron size particles are usually obtained through the gel routes

tion for the formation of Y-123 goes to almost completion at this temperature. The lower reaction temperatures in these two cases is due to the very fine particles of their respective precursor powders.

The particle size distribution of precursor powders are shown in Fig. 4. The particle sizes of precursor powders are in the submicron range. The phases identified by XRD of the samples after various heat treatments and the lattice parameters evaluated from the diffraction patterns of the oxygenated samples of Y-123 phase are presented in Table 2.

The XRD patterns of the samples heat treated at 1173 K/24 h in air are shown in Fig. 5. An impurity phase Y_2BaCuO_5 (Y-211) is formed in the sample prepared by acetate gel, whereas traces of $BaCuO_2$ are observed in the XRD patterns of both the samples prepared from acetate-citrate and nitrate-citrate gel routes. However, at this temperature, a phase pure Y-123 compound is formed through the acrylamide gel route. Superconducting properties of Y-123 prepared by various gel routes are summarised in Table 3.

Kinetics and mechanism of formation of $YBa_2Cu_3O_{7-\delta}$

The mass loss data above 973 K are analysed because formation of perovskite and other phases generally takes place above this temperature. The mass loss data is normalised to α. The parameter $\alpha = W_T/W_\infty$, where W_T is the mass loss at the temperature T (i.e. the difference between the initial mass and the mass of the sample at T) and W_∞ is the maximum mass loss (i.e. difference between the initial and final mass) is evaluated. Figure 6 shows the variation of the parameter α with the temperature. From this data, the differential thermogravimetry (DTG) plots are obtained for all the samples. The DTG peak positions of all the gel samples are presented in the Table 4.

Figure 7 shows the DTG peaks obtained for various gel samples. In the acetate gel samples, the mass loss occurs in two steps leading to two DTG peaks, whereas

Table 2 Phases formed in various gel samples at different temperatures

S. No.	Gel route	Phases formed at different temperatures			Lattice parameters/Å
		Gel decomposition temperature	1173 K/ 24 h in air	1223 K/ in oxigen	
1	Acetate	698-Y_2O_3, $BaCO_3$ and CuO	Y-123, Y-211	Y-123, Y-211	3.845, 3.871, 11.657
2	Nitrate-citrate	698-Y_2O_3, $BaCO_3$ and CuO	Y-123, $BaCuO_2$ (traces)	Y-123	3.813, 3.875, 11.650
3	Acetate-citrate	724-Y_2O_3, $BaCO_3$ and CuO	Y-123, $BaCuO_2$	Y-123	3.825, 3.875, 11.650
4	Acrylamide	778-Y_2O_3, $BaCO_3$ CuO and Y-123	Y-123	–	3.808, 3.880, 11.678

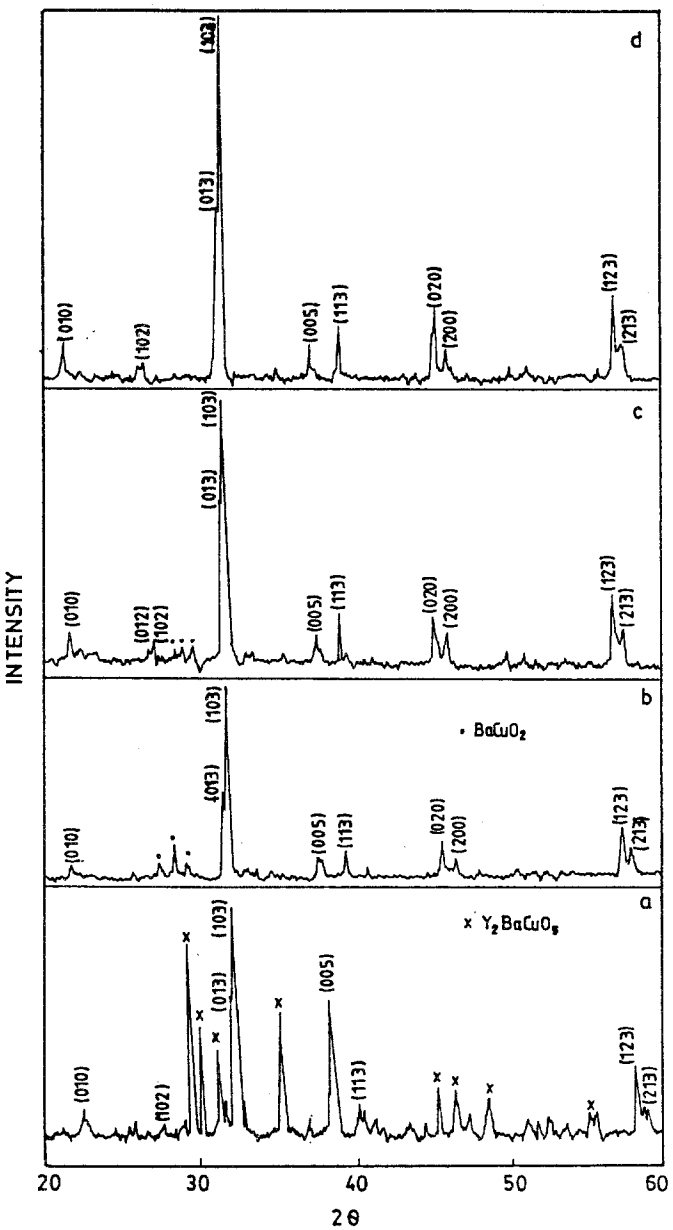

Fig. 5 XRD of the samples showing the formation of Y-123 when heat treated at 1173 K/24 h in air a) acetate, b) acetate-citrate, c) nitrate-citrate and d) acrylamide. A single phase Y-123 is formed through acrylamide gel route

gels derived from other routes show single step mass loss resulting in one DTG peak with discrete shoulders in some cases.

Table 3 Superconducting transition temperatures, normal state resistivity, T_c and oxygen contents of Y-123 samples derived from various gel routes

S. No.	Sample	$T_{c,zero}$/ K	ΔT_c/ K	ρ_{300K}/ mΩ cm	ρ_{150K}/ mΩ cm	T_c/ χ–T	Oxygen content	Superconducting vol. fraction/ %
1	Acetate	79	2.7	26.80	19.80	67	6.75	52
2	Acetate-citrate	90	3.0	13.82	10.50	90	6.88	64
3	Nitrate-citrate	91	2.7	10.80	6.07	90	6.90	65
4	Acrylamide	90	1.2	7.40	4.52	92	6.96	75

Figure 8 shows the XRD patterns of the samples quenched from DTG peak temperatures. The phases identified by the XRD at corresponding DTG peak temperatures are shown in Table 4. The single DTG peak that appear for acetate-citrate, nitrate-citrate and acrylamide gels are due to the formation of Y-123 phase (Fig. 8). In case of acetate gel, the first DTG peak is due to the formation of $BaCuO_2$ and the second DTG peak is due to the formation of Y-123 (Fig. 8).

A method proposed by Phadnis and Deshpande [19] is used to find out the probable mechanism responsible for the Y-123 phase formation. According to this method $f(\alpha)g(\alpha) = RT^2/E(d\alpha/dT)$ where $f(\alpha)$ is the function related to the reaction mechanism and $g(\alpha)=\int d\alpha/f(\alpha)$ and other terms have their usual meanings. Each reaction mechanism has a specific form of $f(\alpha)$. The function relating to various reaction mechanisms have to be incorporated in the above equation to generate the plots of $f(\alpha)g(\alpha)$ *vs.* $T^2(d\alpha/dT)$ for the respective mechanisms. The mechanism exhibiting a linear behaviour in the above plots is considered as the mechanism responsible for the reaction process. The activation energies are estimated from the following relation $g'(\alpha)=-E/RT$, where $g'(\alpha)=\int d\alpha/f(\alpha)g(\alpha)$. In the present investigation $f(\alpha)g(\alpha)$ *vs.* $T^2 d\alpha/dT$ and $g'(\alpha)$ *vs.* $1/T$ plots are generated for various mechanisms viz., Power law, Nucleation and nuclei growth (Mampel's random nucleation, Avrami-Erofeev nuclei growth and Prout-Tomkins branching nuclei), Diffusion controlled (Jander, 3-dimensional diffusion, Anti-Jander 3-dimensional counter diffusion, Brounshtein-Ginstling 3-dimensional diffusion and Valensi, 2-dimensional diffusion) exponential, Phase boundary (contracting sphere, cylinder) and Reaction order.

Table 4 DTG peak temperatures of gels and the phases formed at these temperatures

S. No.	Gel route	Temperature/K	Phases
1	Acrylamide	1096	123
2	Nitrate-citrate	1128	123 and $BaCuO_2$
3	Acetate-citrate	1195	123 and $BaCuO_2$
4	Acetate	1063	$BaCuO_2$, $BaCO_3$, Y_2O_3 and CuO
		1148	123, $BaCuO_2$ and 211

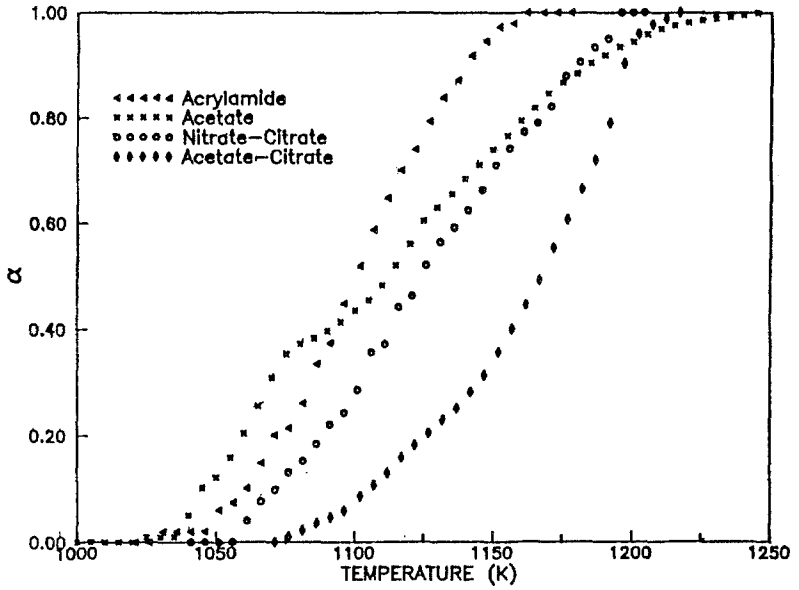

Fig. 6 α–*T* plots of gels indicating that the reaction is complete at a lower temperature in acrylamide gel

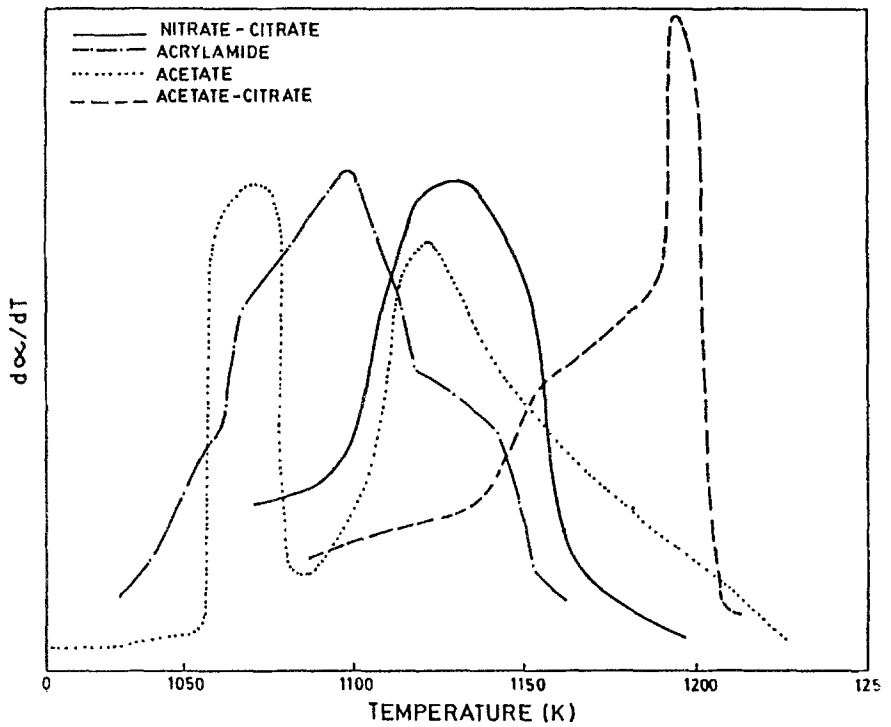

Fig. 7 DTG peaks for gels showing the reaction temperature for phase formation

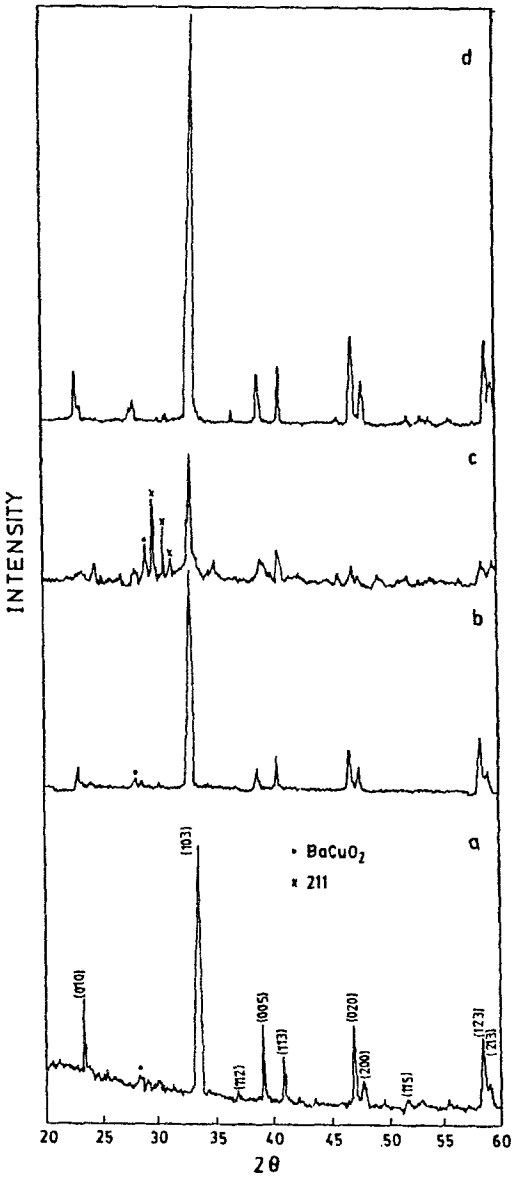

Fig. 8 XRD patterns of the samples quenched from DTG peak temperatures for the samples a) acetate-citrate, (1195 K), b) nitrate-citrate (1128 K), c) acetate (1148 K) and d) acrylamide (1096 K)

Acrylamide route

TG data show only one step mass loss during the formation of Y-123 phase. The DTG peak is found to be at 1103 K. The XRD patterns of the samples quenched

from this temperature show the formation of Y-123 compound. In fact traces of Y-123 compound are observed even in the samples quenched from 883 K (Fig. 3). The absence of the phase transformation peak of $BaCO_3$ in DTA, traces of Y-123 compound in the sample quenched from 883 K and the complete formation of the 123 compound at 1103 K heat treated sample confirms that Y-123 phase formation occurs at much lower temperatures in the acrylamide gel route. From the reaction sequence proposed for the formation Y-123 compound by Ruckenstein *et al.* [20], the probable reaction sequence for the formation of Y-123 is as follows:

$$Y_2O_3 + 4BaCO_3 + 6CuO \rightarrow 2YBa_2Cu_3O_{6.5} + 4CO_2 \quad (1)$$

The expected mass loss for the above reaction is around 11.3%, which matches the observed mass loss of 11.48% in the TG curve.

Figure 9 shows the $f(\alpha)g(\alpha)$ plots for determining the mechanism of formation of Y-123. In these plots linear behaviour is obtained only for the Avrami-Erofeev nuclei growth mechanism. This nucleation process involves the conversion of a small volume of the reactants into a stable product particle and continued reaction (growth) occurs at the interface between the reactants and the products. The growing nuclei overlap during heating and a continuous solid product layer is formed. The compositional uniformity of the individual precursor particles has the greatest impact on the rate of Y-123 production [21]. Since the precursor powder contains very fine particles of $BaCO_3$ which are uniformly surrounded by the Y_2O_3 and CuO, the diffusion process is not a rate determining step. The activation energy estimated from the $g'(\alpha)$ plots (Fig. 10) is 50 kJ mol^{-1}, which is quite low compared to the literature value of 250 kJ mol^{-1} [8, 9]. This is due to the extremely fine particles (0.5 μm) of the precursor powders and homogeneous distribution of reactants.

Nitrate-citrate route

TG data shows only one step mass loss. The XRD pattern of the samples quenched from DTG peak temperatures show the presence of both Y-123 phase and traces of $BaCuO_2$ phase. The mass loss observed may be due to the formation of both of these phases. The Y-123 phase forms through Eq. (1) and the probable reaction for the formation of $BaCuO_2$ is as follows:

$$BaCO_3 + CuO \rightarrow BaCuO_2 + CO_2 \quad (2)$$

The mass loss observed from the TG curve is 9.22% which is lower than the expected loss for the Eq. (1). This may be due to the $BaCuO_2$ formation at 773 K (Fig. 3) consuming a part of $BaCO_3$. The formation of Y-123 compound may also occur through the following reaction

$$4BaCuO_2 + 2CuO + Y_2O_3 \rightarrow 2YBa_2Cu_3O_{7-\delta} \quad (3)$$

Since the $BaCuO_2$ phase is present in traces (Fig. 8) in the sample quenched from the DTG peak temperature, the Y-123 compound mainly forms by Eq. (1).

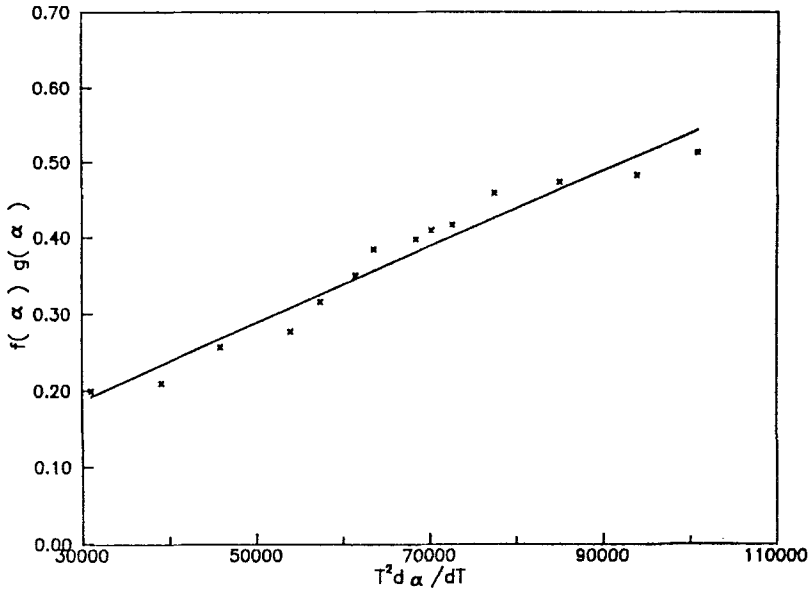

Fig. 9 $f(\alpha)g(\alpha)$ *vs.* $T^2 d\alpha/dT$ plots for gels from acrylamide route showing the Avrami-Erofeev nuclei growth mechanism is responsible for Y-123 formation

The $f(\alpha)g(\alpha)$ plot for the nitrate-citrate sample is shown in Fig. 11. The linear behaviour is observed only for diffusion controlled processes following Ginstling's kinetics. The diffusion controlled process can be explained by unreacted-core-shrinking model [22, 23]. Consider the reaction, A+B → C, one of the reactant B diffuses through an outer layer of product C and then reacts with A in the inner core. The product layer becomes thicker and thicker while the unreacted core shrinks progressively with time. If the chemical reaction is very rapid and the diffusion of reactants through the product layer is relatively slow, the overall reaction rate is limited by the diffusion of the reactant. The zone of the reaction is narrowly confined to the interface between the unreacted core and the product layer. Assuming that the Eq. (1) is responsible for the formation of Y-123, the oxides of yttrium and copper have to diffuse through Y-123 phase to react with $BaCO_3$ in the reaction zone. Since the ionic radius of Y^{3+} is 0.93 Å and larger than that of Cu^{2+} (0.69 Å), it can be assumed that the overall reaction is limited by the diffusion of Y^{3+} across Y-123 shell. The activation energy is estimated from the g′ plots (Fig. 10) and found to be 416 kJ mol^{-1} which is quite high compared to the reported values [8, 9].

Acetate-citrate

The DTG plots of acetate-citrate samples are shown in Fig. 7. The rate of mass loss is initially sluggish and accelerates at around 1170 K. The samples quenched from DTG peak temperatures show the formation of both Y-123 and $BaCuO_2$ phases. The sluggishness of the reaction in the initial stages is due to non-availabil-

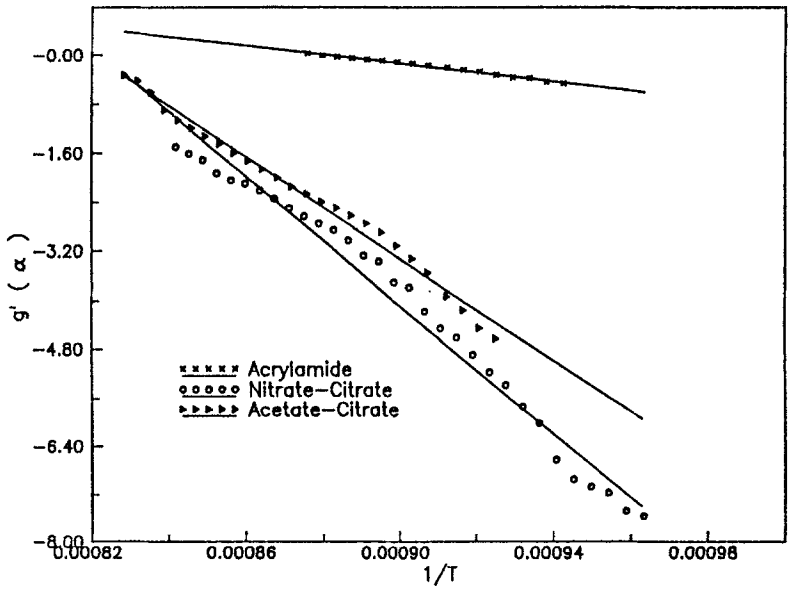

Fig. 10 $g'(\alpha)$ *vs.* $1/T$ for acrylamide, nitrate-citrate and acetate-citrate samples. The slopes of these plots are used to estimate the activation energy for phase formation

ity of escape paths for the CO_2 liberated during the reaction. At lower temperatures, the product formed envelops the unreacted core thereby restricting the escape of CO_2 [9, 24]. However, at higher temperatures, the acceleration in reaction indicates that the rate of diffusion of either reactants or CO_2 is very high. The $f(\alpha)g(\alpha)$ plots are obtained from the mass loss data and are shown in Fig. 12. A linear behaviour is observed for the phase boundary controlled reaction. It is evident that in acetate-citrate gel route, Y-123 compound formation occurs following the phase boundary controlled reaction. The acceleration of the reaction at higher temperatures (as observed from DTG plots) may be due to rapid diffusion of the reactants. When the diffusion through the product layer is rapid enough that reactants can not combine fast enough at the reaction interface to establish equilibrium, then the process becomes phase boundary controlled [22].

A phase boundary controlled interface reaction usually shifts to a diffusion controlled reaction as the reaction proceeds. In the present case, the precursor powders are highly reactive due to their submicron particle size. The reaction is therefore almost complete before diffusion becomes a rate determining step. The activation energy estimated from the g' plots (Fig. 10) is 326 kJ mol^{-1}.

Acetate route

TG plots for these samples show that the mass loss occurs in two steps. From XRD studies it is identified that the first step of mass loss is due to the formation of $BaCuO_2$ and that of the second step is due to the formation of Y-123 and Y-211 phases. During the second step, the rate of mass loss is slightly sluggish in acetate

gel sample compared to other samples (Fig. 6). The escape paths for CO_2 during its formation depends on the homogeneity of the sample. The sluggishness in mass loss

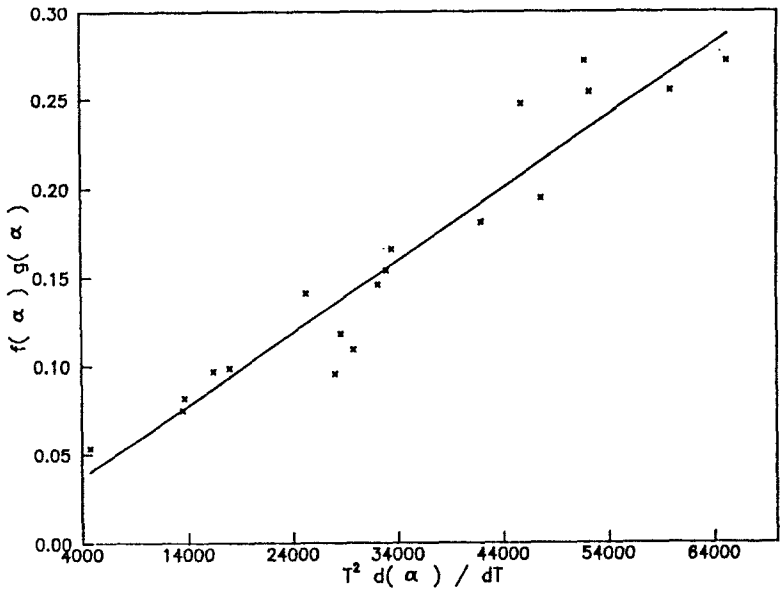

Fig. 11 $f(\alpha)g(\alpha)$ *vs.* $T^2 d\alpha/dT$ for nitrate-citrate gels. The plot indicates that diffusion controlled process following Brounshtein Ginstling – 3-dimensional kinetics is found to be responsible for formation Y-123

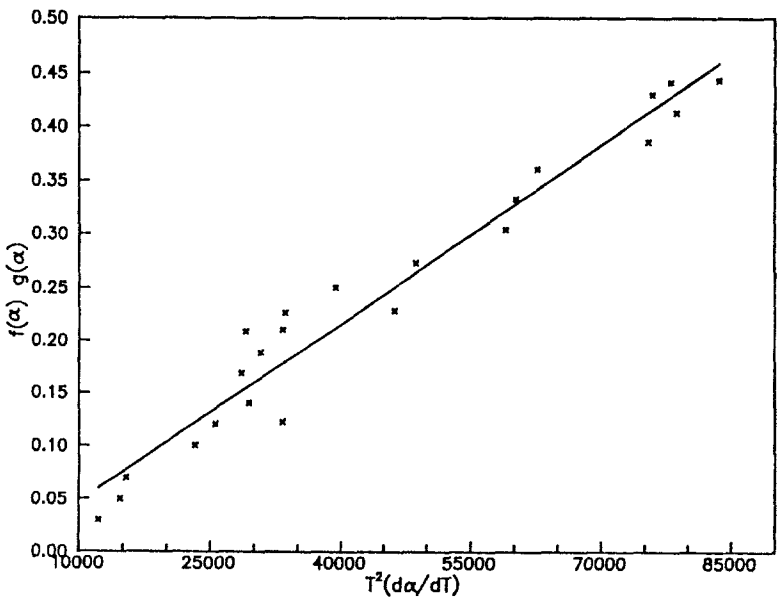

Fig. 12 $f(\alpha)g(\alpha)$ *vs.* $T^2 d\alpha/dT$ for acetate-citrate sample

observed in sample C during the second stage of mass loss may be due to the incomplete escape of CO_2. Because $BaCuO_2$ formed during the first step envelops the unreacted core thereby slowing down the escape of CO_2 [9, 24]. XRD analysis of the samples quenched at the respective DTG temperatures reveal that, together with Y-123, other phases such as Y-211 and $BaCO_3$ are also present. It is observed from the XRD patterns that Y-211 phase persists even in samples heat treated at 1173 K for 24 h in air followed by oxygen treatment at the same temperature for 24 h (Table 2). However, the reflection peaks of $BaCO_3$ are not observed in the XRD patterns, indicating the complete elimination of $BaCO_3$. The probable reaction sequence for the formation of Y-123 and Y-211 phases are as follows:

$$Y_2O_3 + BaCO_3 + CuO \rightarrow Y_2BaCuO_5 + CO_2(g) \quad (4)$$

$$Y_2BaCuO_5 + 3BaCO_3 + 5CuO \rightarrow 2YBa_2Cu_3O_{7-\delta} \quad (5)$$

The formation of Y-211 phase may also take place by the interaction of carbon dioxide with Y-123 compound following a reversal Eq. (5) [25], because the localised concentration of carbon dioxide produced by Reaction (1) might increase during the course of reaction and react with Y-123 to form Y-211 phase [25]. The various impurity phases found in the sample may be the result of several side reactions leading to conclusion that sample is highly inhomogeneous. This may be the reason for its lower superconducting onset transition temperature 79 K, whereas samples prepared through other gels have the onset of superconducting transition temperature at 90 K. From the above discussion the probable reaction sequence for the formation of Y-123 and Y-211 are Reactions (1), (3), (4), (5) and the following Reaction (6):

$$BaCuO_2 + Y_2O_3 \rightarrow Y_2BaCuO_5 \quad (6)$$

The plots of $f(\alpha)g(\alpha)$ *vs.* $T^2 d\alpha/dT$ for the formation of $BaCuO_2$ compound have not shown linear behaviour for any of the mechanisms mentioned earlier. This leads to the conclusion that the reaction processes for the formation of $BaCuO_2$ are quite complex in nature for these samples. Since there are several side reactions during the second step of mass loss, kinetic analysis is not carried out.

Conclusions

The thermoanalytical studies on the influence of various gel routes on the formation of $YBa_2Cu_3O_{7-\delta}$ have led to the following conclusions:

1. The homogeneous distribution of metal ions in the acrylamide and nitrate-citrate gels and the fine reactive powders obtained on gel decomposition lead to the formation of phase Y-123 at lower temperatures (1103–1130 K).

2. The samples prepared through acrylamide, nitrate-citrate and acetate-citrate route showed a single step mass loss for the formation of Y-123 compound.

3. The samples prepared through acetate gel route are highly inhomogeneous results in multistep mass loss leading to formation of maximum percentage of impurity phases and thus affecting the superconducting transition temperature.

4. The steps involved in the formation of Y-123 and the corresponding reactions are identified in various gel routes.

5. Avrami's nuclei growth in case of acrylamide, diffusion controlled process in nitrate-citrate and phase boundary reaction mechanisms in case of acetate-citrate gels are found to be responsible for the formation of Y-123 phase.

* * *

The authors are grateful to Dr. Baldev Raj, Director, Metals and Materials Group, for his constant encouragement and support. We thank Prof. G. V. Subba Rao, Director, Central Electrochemical Research Institute, Karaikudi for his keen interest in this work. Thanks are also due to Dr. Sundaram, CECRI, Karaikudi for his help in thermal analysis experiments.

References

1 U. V. Varadaraju and G. V. Subba Rao in A. V. Narlikar, (Ed.) Studies of High Temperature Superconductors, Nova Science Publishers, New York 1989, p. 229.
2 M. Nagano and M. Greenblatt, Solid State Commun., 67 (1988) 595.
3 J. M. Tarascon, P. B. Barboux, B. G. Bagley, L. H. Greene and G. W. Hull, Mater. Sci. Eng., B 1 (1988) 29.
4. H. Kozuka, T. Umeda, J. Jin, T. Monde and S. Sakka, Bull. Inst. Chem. Res. Kyoto Univ., 66 (1988) 80.
5 G. V. Rama Rao, D. S. Suryanarayana, U. V. Varadaraju, G. V. N. Rao and S. Venkadesan, J. Alloys and Compounds, 217 (1995) 200.
6 G. V. Rama Rao, D. S. Suryanarayana, U. V. Varadaraju, S. Geethakumari and S. Venkadesan, Mater. Chem. Phys., 39 (1994) 149.
7 S. I. Hirano and T. Hayashi, Thermochim. Acta, 174 (1991) 169.
8. M. Kamimoto, Thermochim. Acta, 174 (1991) 153.
9 N. L. Wu and Y. C. Chang, Thermochim. Acta, 203 (1992) 339.
10 J. Šesták and N. Koga, Thermochim. Acta, 203 (1992) 321.
11 A. Gaddala and T. Hegg, Thermochim. Acta, 145 (1989) 149.
12 T. Ozawa, Thermochim. Acta, 133 (1988) 11.
13 M. Kamimoto and T. Ozawa, Thermochim. Acta, 148 (1989) 219.
14 X. P. Jiang, J. S. Zhang, J. G. Huang, M. Jiang, G. W. Qiao, Z. Q. Hu and C. X. Shi, Mater. Lett., 7 (1988) 250.
15 Y.G. Metlin and Y. D. Tretyakov, J. Mater. Chem., 4 (1994) 1659.
16 C. N. R. Rao, R. Nagarajan and R. Vijayaraghavan, Sup. Cond. Sci. Tech., 6 (1993) 1.
17 G. V. Rama Rao, P. V. Sivaprasad, R. K. Singh Raman, S. Venkadesan, S. L. Mannan and U. V. Varadaraju, Thermochim. Acta, 230 (1993) 207.
18 M. I. Pope and M. D. Judd, Differential Thermal Analysis, A Guide to the Technique and its Applications, Heydon and Sons Ltd., London 1977, p. 24.
19 A. B. Phadinis and V. V. Deshpande, Thermochim. Acta, 62 (1983) 361.
20 E. Ruckenstein, S. Narain and N. L. Wu, J. Mater. Res., 4 (1989) 361.
21 V. Minopoulou, K. M. Forster, J. P. Formica, J. Kulik, J. T. Richardson and D. Luss, J. Mater. Res., 9 (1994) 275.
22 J. Šesták, V. Satava and W. Wendlandt, Thermochim. Acta, 7 (1973) 333.
23 N. L. Wu, T. C. Wei, S. Y. Hou and S. Y. Song, J. Mater. Res., 5 (1990) 2056.
24 U. A. Tamburini, P. Ghigna, G. Spinolo and G. Flor, J. Phys. Chem. Solids, 52 (1991) 715.
25 G. Selvaduray, C. Zhang, U. Balachandran, Y. Gao, K. L. Merkle, H. Shi and R. B. Poeppel, J. Mater. Res., 7 (1992) 283.